Mitigation of nonlinear phase noise in coherent 16-QAM long-reach PONs by K-nearest neighbors-based classification

Rômulo de Paula, Lúcio Neri Borges, Marcelo Luis Francisco Abbade, and Ivan Aldaya

***Abstract*— Nonlinear phase-noise induced by the Kerr effect is the main nonlinear impairment in single-channel coherent long-reach passive optical networks (LR-PONs). In this work, we explore the capability of the K-nearest neighbors (KNN) algorithm to mitigate this impairment in links with non-negligible fiber dispersion. Simulation results show that when employing KNN in a 56-Gbps coherent LR-PON with a 100-km range and 1:64 splitting ratio, the effective Q-factor is improved by 0.15 dB with respect to maximum likelihood. This increment is achieved by setting the parameter *K* to 13, which leads to a minimum training data set size of 500 symbols.**

***Keywords*— Coherent optical communications; Passive optical networks; Nonlinear phase noise; Machine learning; K-nearest neighbors.**

I. Introduction

Due to their high capacity-distance product, optical fiber links have been adopted not only for long-haul but also for lower-range applications [1]. For decades, intensity modulation with direct detection (IM/DD) systems could meet the increasing throughput requirements but, with the popularization of multimedia applications and migration to cloud services, these systems are becoming obsolete [2]. In this context, the introduction of coherent receivers employing digital signal processors (DSPs) gave birth to the fifth generation lightwave systems. These systems allowed to retain not only phase but also polarization information, thus enabling the utilization of advanced modulation formats with unprecedented spectral efficiency [3]. In addition, the adoption of high performance forward error correction (FEC) codes enabled the increase of the number of points in the constellation, leading to M-ary phase shift keying (PSK), quadrature phase shift keying, and quadrature amplitude modulation (QAM).

In digital coherent systems, linear impairments such as chromatic dispersion (CD), polarization mode dispersion (PMD), and linear phase noise can be compensated using well-established DSP algorithms [4] [5]. On the other hand, the reduction of Kerr-induced nonlinear distortion remains as an open problem. In this work we focus on single channel systems with unrepeated links, i.e. long reach passive optical networks (LR-PONs), where no cross-phase modulation (XPM) or four wave mixing (FWM) are present and, therefore, self-phase modulation (SPM) is the dominant nonlinear distortion mechanism [1]. Besides the nonlinear distortion, the absence of mid-span amplifiers and the high transmission loss, makes the noise produced by the photodetector to result in a low signal-to-noise ratio (SNR). Additionally, even if accumulated CD is compensated at the receiver, significant intersymbol interference (ISI) is present along the fiber. The overlap of adjacent symbols then results on a stochastic-like behaviour of the SPM, as it depends on the local intensity [6]. Therefore, the mitigation of the harmful distortion caused by the complex interplay among the SPM and ISI that results in nonlinear phase noise (NLPN), in combination with the receiver noise, becomes challenging, specially in multi-level modulation formats where higher amplitude symbols are more affected.

Some methods for nonlinear impairments has already been proposed, both in the optical and electrical domains. In the optical domain, two of the methods that attracted more attention are conjugated twin-waves [7] and mid-span conjugation [8]. These methods, however, suffer from either low flexibility or reduced capacity. In the electrical domain, on the other hand, the flexibility of digital electronics enables adaptive nonlinear compensation. The traditional electronic approach for nonlinear impairment compensation relay on model inversion, for instance, digital backward propagation (DBP) [9], inverse Volterra-series transfer function (IVSTF) [10] and Wiener Hammerstein (WH) [11], [12]. One of the advantages of these methods is that they are modulation format agnostic, thus showing flexibility in systems where adaptive modulation is used. Unfortunately, the elevated computational cost of model inversion prevents their adoption in real-time applications. In this context, machine learning has emerged as a feasible lower complexity alternative with high potential for implementation in future nonlinear mitigation schemes.

Machine learning algorithms can be roughly divided into supervised and unsupervised [13]. Unsupervised algorithms include clustering, as in [14] and [15], in which constellation symbols are classified utilizing histogram based clustering and expectation maximization, respectively. On the other hand, supervised algorithms require a training set in which both the data and their labels are previously known by the receiver. Supervised algorithms can perform either regression or classification, depending whether the output is discrete or continuous. In [16], an artificial neural network (ANN) is used as an equalizer to compensate SPM in optical links, whereas in [17] and [18], support vector machines (SVM) and K-nearest neighbors (KNN) algorithms are proposed for

Campus São João da Boa Vista, Universidade Estadual Paulista "Júlio de Mesquita Filho" - Unesp, São João da Boa Vista - SP, e-mails: romulo.junior314@yahoo.com.br, lucio.borges@unesp.br, marcelo.abbade@unesp.br, ivan.aldaya@unesp.br.

supervised classification, respectively. As a lazy algorithm, K-nearest neighbors (KNN) does not require to fit a set of parameters to a training sequence [19], leading to an extremely simple learning process [18]. Therefore, it is a good solution for flexible systems where training has to be fast. Nevertheless, to the best of our knowledge, KNN algorithm has not been yet tested in links employing standard single mode fibers (SSMF) where the dispersion parameter is around 16 ps/(km·nm).

In this work, we numerically implement and optimize a KNN-based classifier to mitigate the nonlinear effects (NLPN) caused by SPM on a 16-QAM digital coherent optical system. The rest of the paper is organized as followed: Section II describes the fundamentals of KNN, in Section III, we describe the simulation setup used in this work, Section IV discusses the obtained results, and Section V concludes our work.

II. K-NEAREST NEIGHBORS

As a supervised classification algorithm, KNN requires a training data set of size N_{tr}, where each received symbol is represented by an N-dimensional feature vector $\mathbf{x}^{(i)}$ and its label, which is a natural constant $y^{(i)}$ indicating its class. Thus, in KNN, training process consists in just storing the set of training symbols and their respective labels, $\{\mathbf{x}^{(i)}, y^{(i)}\}$, $1 \leq i \leq N_{tr}$, for subsequent comparison.

When a new symbol with features $\mathbf{x}^{(j)}$ is received, its Euclidean distances $d_{i,j}$ to all the stored training symbols $\mathbf{x}^{(i)}$ are computed employing:

$$d_{i,j} = d\left(\mathbf{x}^{(i)}, \mathbf{x}^{(j)}\right) = \sqrt{\sum_{n=1}^{N} \left(x_n^{(i)} - x_n^{(j)}\right)^2}, \qquad (1)$$

where subindex n indicates the n-th component of the feature vector. After calculating the distance to all the training symbols, the K symbols with shortest $d_{i,j}$ are selected, hence the name *K nearest neighbors*. The most common class among the neighbor symbols is then assigned to $\mathbf{x}^{(j)}$. To avoid a tie in decision, the parameter K must be odd in binary classification but there is not such a restriction for multi-class classification problems.

In Fig. 1, we show an example of the KNN-based classification of a 16-QAM constellation with a training set of 35 symbols per class. Then, a total number of 560 symbols were used for illustration purposes. The symbols are labeled from 1 to 16, which are represented in the plot from the left-to-right and top-to-bottom. A K of 13 was chosen, meaning that the 13 nearest symbols will be used for the classification of the example symbol that is identified with a star marker. As can be seen, the example symbol is located in the vicinity of the symbols corresponding to the classes 3, 4, 7, and 8. The length of the lines from the example symbol represent the distances between it and the 13 nearest symbols, while the radius of the circle around it shows the distance to the farthest K nearest symbol. To facilitate the interpretation of the KNN classification method, a table including the distances to the K nearest neighbors and their associated classes is included. As shown, most of the the K symbols with shortest distance belong to class 3 and, consequently the example symbol will be labeled as class 3.

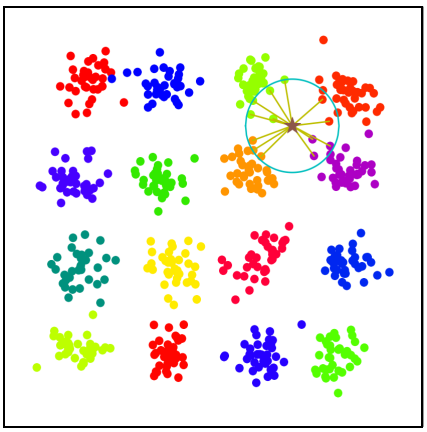

Points	Distance	Class
1	0.151	3
2	0.182	8
3	0.278	4
4	0.278	8
5	0.299	4
6	0.311	3
7	0.315	7
8	0.321	8
9	0.322	3
10	0.326	7
11	0.344	7
12	0.349	3
13	0.349	3
Statistical Mode:		3

Fig. 1. KNN classification with K = 13 of a new incoming symbol identified by a star marker. The adjacent table indicates the distance and the class of the k nearest symbols.

Another point to highlight about the KNN simplicity is that it depends only on a single model parameter, K, which is set before the training stage. However, the size of training set is also an important factor to be considered, as this impacts both the performance and the complexity of the classification. Thus, if the algorithm requires a low number of training symbols, N_{tr}, we will have a shorter overhead and higher information throughput. In Section IV, we study the effect of both K and N_{tr} on the system performance to find their optimum values.

III. SIMULATION SETUP

Fig. 2 shows the setup relying on co-simulation between Matlab and VPI Transmission Maker. This setup was used to evaluate the KNN classification in a LR-PON utilizing 16-QAM modulation. Due to its flexibility, Matlab was adopted to implement the electrical modulation, DSP, and demodulation

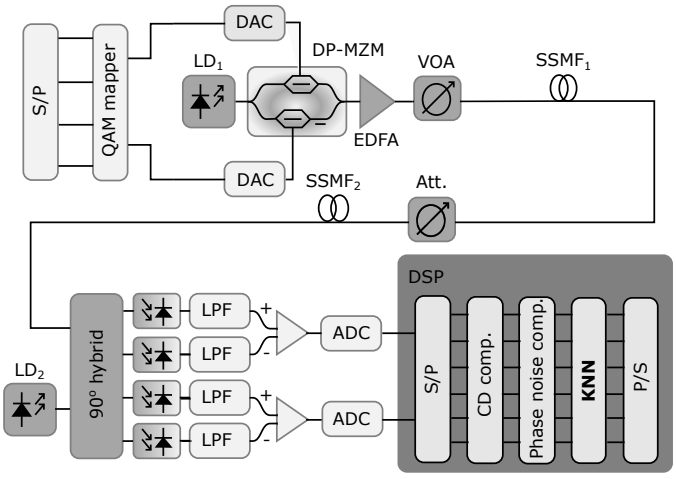

Fig. 2. Illustration of the simulated coherent LR-PON system. S/P: serial-to-parallel conversion. DAC: digital to analog converter. LD:laser diode. DP-MZM: dual parallel-Mach-Zenhder modulator. EDFA: erbium-doped fiber amplifier. VOA: variable opticalattenuator. SSMF: standard single mode fiber. Att: attenuator. LPF: low-pass filter. ADC: analog-to-digital converter. DSP:digital signal processing.

stages, while VPI Transmission Maker was used to simulate the electrical-to-optical conversion, fiber transmission, and signal detection.

The system performance was assessed comparing the bit error ratio (BER) and the effective Q factor of the proposed classification method with those obtained using the commonly adopted maximum likelihood (ML). Due to the non-Gaussian distribution of the constellation points, the BER was computed by error counting, and the Q factor was obtained from the BER, by inverting the expression $BER = 1/2 \cdot erfc(Q/\sqrt{2})$, where $erfc$ represents the complementary error function [20].

In the transmitter, the first stage consisted in a serial-to-parallel conversion of the incoming 56-Gbps bit stream to 4-bit blocks for mapping into a 16-QAM constellation. The in-phase and quadrature components of the mapped symbols were oversampled to emulate the digital-to-analog conversion and employed to drive the dual parallel Mach–Zehnder modulator (DP-MZM). This DP-MZM was used to modulate a continuous wave (CW) laser with a linewidth of 100 kHz and an emission power of 1 mW operating at 1550 nm. The power of the modulated signal was boosted by an erbium-doped fiber amplifier (EDFA), which had an output of 13 mW. Since the EDFA gain was not too high, no significant amount of amplified spontaneous emission noise was added. Finally, a variable optical attenuator (VOA) was used to sweep the power at the input of the distribution network from 2 to 13 mW.

The distribution network was formed by an 80-km-length standard single mode fiber (SSMF) link, an 18-dB attenuator representing the splitting loss of the signal to 64 users, and a second link of SSMF with a length of 20 km.

At the receiver front-end, the incoming signal was first mixed with a 1-mW CW local oscillator laser employing a 90º optical hybrid network. The corresponding in-phase and quadrature components of the received signal were converted to the electrical domain by utilizing two pairs of balanced photodetectors, whose bandwidth response was modeled by a 4th-order electrical Bessel filters.

At the DSP, the first module carried out the compensation of the CD in the frequency-domain. The time synchronization stage relied on a pilot sequence of 64 symbols of alternating amplitudes, optimizing the sampling times by the method of cross-correlation maximization. A downsampling process was then performed to get a single sample per symbol. Through a blind search algorithm, the stochastic phase rotation caused by the combined phase noises of both transmitter and receiver laser diodes was compensated. It is worth mentioning that, as the total length of the link was 100 km, the accumulated PMD is significantly smaller than the symbol period and, consequently, it did not require compensation. After overhead removal, 81,500 data symbols were available. These symbols were divided in a training set of up to 10,000 symbols and a fixed test set of 71,500 symbols. The signal quality was assessed considering the bit error ratio (BER) calculated by error counting, whereas as mentioned the performance improvement of the KNN classification method was quantified comparing the BER at optimum launch optical power for KNN and the that of ML.

IV. Results and Discussion

A. Performance analysis

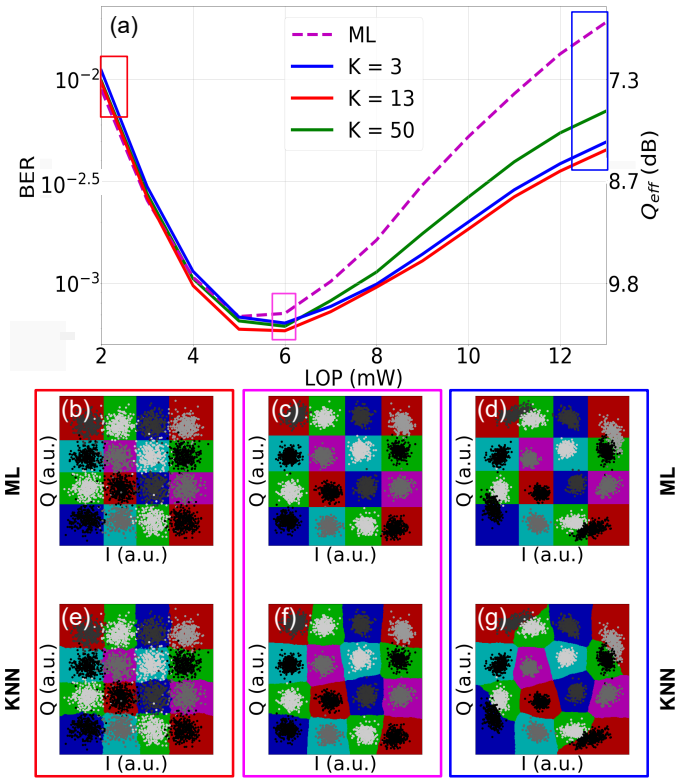

Fig. 3. Performance analysis. (a) BER obtained using ML and KNN in terms of the launch optical power. For KNN three different configurations are considered: K = 3, 13, and 50. (b-d) Received constellations alongside with the obtained decision regions for ML at 2, 6, and 13 mW. (e-f) The same as (b-d) but for KNN classification.

Fig. 3(a) shows the BER obtained when the received symbols are classified utilizing ML and KNN methods. To ensure optimum performance of KNN, we swept the value of K, i.e. the number of neighbors to be considered, obtaining an optimum of K = 13. Nevertheless, in Fig. 3(a) we present the results for K = 3, 13, and 50 to show the performance of choosing a small, an optimum, and a large value of K. As can be observed, at low power levels, where the dominant impairment is the additive noise, the BER obtained employing both methods is similar, regardless of the configuration of KNN. As we increase the launch optical power (LOP), KNN progressively outperforms ML. This point can be seen at intermediate LOPs where NLPN begins to be appreciable but is specially notorious at higher values of LOP. As a result of the partial nonlinearity mitigation, it is possible to reduce the optimal BER from $7.12{\cdot}10^{-4}$ obtained using ML to $6.37{\cdot}10^{-4}$, $5.85{\cdot}10^{-4}$, and $6.15{\cdot}10^{-4}$ when adopting KNN with K = 3, 13, and 50, respectively. This system performance improvement corresponds to a 0.15-dB increase in the effective Q-factor. In addition, for a forward error correction (FEC) threshold of $2 \cdot 10^{-3}$, by employing KNN, the transmission power limit can be increased from 8 mW to 10 mW, which represents a $\approx$ 1 dB gain in the power margin.

In order to see why KNN-based classification presents a better performance than ML, in Fig. 3(b-d) we illustrate the constellations alongside with the decision regions using ML at LOPs of 2, 6, and 13 mW, respectively. As can be seen, when using ML, the boundaries of the decision regions are straight and orthogonal, which are suitable for low power levels but are not optimum for high LOPs. Fig. 3(e-g), on the other hand, represent the same constellations but employing a KNN classifier instead of ML. At low level powers, KNN and ML traced similar boundaries and, consequently, they lead to almost the same BER values. This can be understood by noting that when the additive noise is dominant, the randomness of the generated pattern avoids the class of new symbols to be predicted based on previously received symbols. At higher values of LOP, the resulted boundaries are not straight anymore. These curved boundaries better fit the dispersion of the points, thus reducing the amount of errors. Such improvement is possible because, even if complicated, the underlying NLPN effect is deterministic and, therefore, a pattern can be found by means of machine learning algorithm.

As mentioned in Section I, in multi-level modulation formats, NLPN affects more strongly symbols with higher intensity. This can be clearly observed in Fig. 3(d) and (g). For the sake of visualization of amplitude-dependent nonlinear impairments mitigation, it is useful to analyze the BER of each class individually rather than its average. Considering this, Fig. 4 represents the BER of each class separately for both ML (a-c) and KNN detection (d-f) at LOPs of 2, 6, and 13 mW. The BER values presented in Fig. 4 can be interpreted as the complimentary of the classification accuracy of the confusion matrix. Looking at the highest LOP, Fig. 4(c) and (f), it is possible to see that the KNN allows to reduce the BER of the symbols with highest amplitude from $5{\cdot}10^{-3}$ to $1.5{\cdot}10^{-3}$, which most contributes to the total BER is given by the classification of the four vertexes symbols. Nevertheless, even if KNN mitigates the effect of NLPN, the vertex symbols of the constellation still present higher BER.

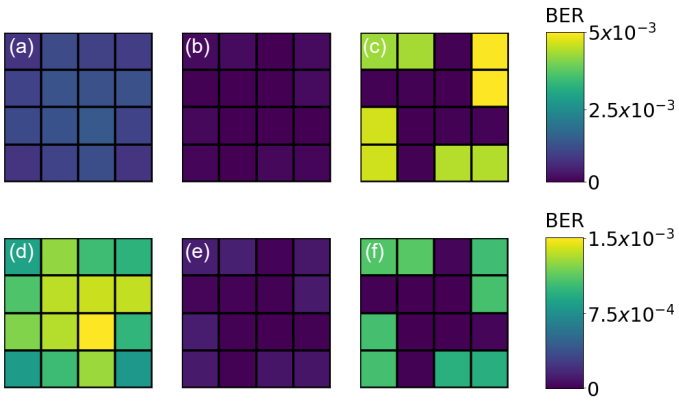

Fig. 4. BER for each class for (a-c) ML detection and (d-f) KNN-based classification with optimum K. Both methods are tested at LOPs of 2, 6, and 13 mW.

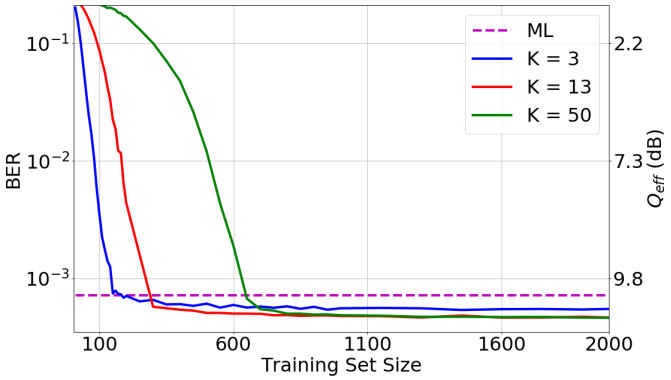

Fig. 5. Calculated BER in terms of the training set size for different values of K, i.e. K=3, 13, and 50. The optimum BER achieved using ML is also included as a benchmark.

B. Training test size analysis

The optical channel in a LR-PON system is relatively static, which means that the training stage is not accomplished frequently. Nevertheless, it is still important to analyze the optimal training set size, to assess the capability of the system to adapt to eventual re-configurations. In Fig. 5, we show the BER convergence curves as a function of the training set size for three KNN configurations: $K = 3$, 13 and 50. In all cases a LOP of 6 mW was considered. Maintaining the test set fixed, the training was performed in subsets of sizes ranging from 10 to 2,000 symbols. Taken into account that different training set examples give different performance results, for each training size we performed the training 50 times by selecting random subsets. As expected, for low training set sizes, the BER is high for all the contemplated configurations. As the training set size is increased, the BER tends to converge. It can be observed that for a small value of K, the algorithms requires a shorter training size to converge. For a higher value of K, as $K = 50$, the convergence is slower but it converges to a smaller BER value. Thus, $K = 13$ presents an optimum tradeoff between convergence and perfomance. For the sake of comparison, the dashed line in Fig. 5 shows the BER achieved when the ML method is used. Hence, we can conclude that for the system under test, a good performance KNN can be achieved with a small N_{tr} and, consequently, with low computational complexity.

V. Conclusions

In this paper we analyzed the capability of KNN for mitigating the effect of the nonlinear phase noise in coherent LR-PONs employing 16-QAM. Simulation results reveal that for a 100-km link with a 1×64 splitting ratio and operating at 56 Gbps, the optimum configuration is achieved for a value of K =13, which results in a Q-factor improvement of 0.15 dB when compared to ML. The effect of the training set size was also investigated, showing that higher values of K require larger training sets. In particular, for K=13, KNN requires approximately 500 symbols to get optimum performance.

ACKNOWLEDGMENTS

The authors thank the National Council for Scientific and Technological Development (CNPq, grant numbers 432303/2018-9 and 311035/2018-3) and the São Paulo Research Foundation (FAPESP, grant 2018/25339-4).

REFERENCES

[1] G. P. Agrawal, "Optical communication: its history and recent progress," in *Optics in Our Time*. Springer, Cham, 2016, pp. 177–199.

[2] C. V. N. Index, "Forecast and methodology 2017–2022," *Cisco: San Jose, CA, USA*, 2019.

[3] P. J. Winzer, "High-spectral-efficiency optical modulation formats," *Journal of Lightwave Technology*, vol. 30, no. 24, pp. 3824–3835, 2012.

[4] D. Lavery, R. Maher, D. S. Millar, B. C. Thomsen, P. Bayvel, and S. J. Savory, "Digital coherent receivers for long-reach optical access networks," *Journal of Lightwave Technology*, vol. 31, no. 4, pp. 609–620, 2012.

[5] D. Lavery, B. C. Thomsen, P. Bayvel, and S. J. Savory, "Reduced complexity equalization for coherent long-reach passive optical networks," *Journal of Optical Communications and Networking*, vol. 7, no. 1, pp. A16–A27, 2015.

[6] M. N. Chughtai, "Nonlinear phase noise in fiber optical communication," Ph.D. dissertation, Chalmers University of Technology, 2009.

[7] C. McKinstrie, S. Radic, and C. Xie, "Reduction of soliton phase jitter by in-line phase conjugation," *Optics Letters*, vol. 28, no. 17, pp. 1519–1521, 2003.

[8] K.-P. Ho, "Mid-span compensation of nonlinear phase noise," *Optics Communications*, vol. 245, no. 1-6, pp. 391–398, 2005.

[9] C.-Y. Lin, R. Asif, M. Holtmannspoetter, and B. Schmauss, "Nonlinear mitigation using carrier phase estimation and digital backward propagation in coherent QAM transmission," *Optics Express*, vol. 20, no. 26, pp. B405–B412, 2012.

[10] L. Liu, L. Li, Y. Huang, K. Cui, Q. Xiong, F. N. Hauske, C. Xie, and Y. Cai, "Intrachannel nonlinearity compensation by inverse Volterra series transfer function," *Journal of Lightwave Technology*, vol. 30, no. 3, pp. 310–316, 2012.

[11] J. Pan and C. Cheng, "Wiener–Hammerstein model based electrical equalizer for optical communication systems," *Journal of Lightwave Technology*, vol. 29, no. 16, pp. 2454–2459, 2011.

[12] J. Torres-Zugaide, I. Aldaya, G. Campuzano, E. Giacoumidis, J. Beas, and G. Castañón, "Range extension in coherent OFDM passive optical networks using an inverse hammerstein nonlinear equalizer," *Journal of Optical Communications and Networking*, vol. 9, no. 7, pp. 577–584, 2017.

[13] S. Shalev-Shwartz and S. Ben-David, *Understanding Machine Learning: From Theory to Algorithms*. USA: Cambridge University Press, 2014.

[14] I. Aldaya, E. Giacoumidis, G. de Oliveira, J. Wei, J. L. Pita, J. D. Marconi, E. A. M. Fagotto, L. Barry, and M. L. F. Abbade, "Histogram based clustering for nonlinear compensation in long reach coherent passive optical networks," *Applied Sciences*, vol. 10, no. 1, p. 152, 2020.

[15] D. Zibar, O. Winther, N. Franceschi, R. Borkowski, A. Caballero, V. Arlunno, M. N. Schmidt, N. G. Gonzales, B. Mao, and Y. Ye, "Nonlinear impairment compensation using expectation maximization for dispersion managed and unmanaged PDM 16-QAM transmission," *Optics Express*, vol. 20, no. 26, pp. B181–B196, 2012.

[16] Y. Fukumoto, S. Owaki, T. Sakamoto, N. Yamamoto, and M. Nakamura, "Experimental demonstration of SPM compensation based on digital signal processing using a complex-valued neural network for 40-Gbit/s optical 16QAM signals," in *23rd Opto-Electronics and Communications Conference (OECC)*, July 2018, pp. 1–2.

[17] D. Wang, M. Zhang, Z. Li, Y. Cui, J. Liu, Y. Yang, and H. Wang, "Nonlinear decision boundary created by a machine learning-based classifier to mitigate nonlinear phase noise," in *European Conference on Optical Communication (ECOC)*. IEEE, 2015, pp. 1–3.

[18] D. Wang, M. Zhang, M. Fu, Z. Cai, Z. Li, H. Han, Y. Cui, and B. Luo, "Nonlinearity mitigation using a machine learning detector based on k-nearest neighbors," *IEEE Photonics Technology Letters*, vol. 28, no. 19, pp. 2102–2105, 2016.

[19] E. Alpaydin, *Introduction of Machine Learning*. The MIT Press, 2014.

[20] R. A. Shafik, M. S. Rahman, and A. R. Islam, "On the extended relationships among EVM, BER and SNR as performance metrics," in *International Conference on Electrical and Computer Engineering*. IEEE, 2006, pp. 408–411.